Developments in Proton Conducting Membranes for Hydrogen Separation and Fuel Cell Applications

Marie-Laure Fontaine[1], Yngve Larring[1], Martin Fleissner[1], Claude Estournès[2], Christian Kjolseth[3], Truls Norby[3], Øystein S. Andersen[4], Kjell Wiik[4], Rune Bredesen[1]

(1) SINTEF, 124 Blindern, N-0314 Oslo, Norway,
(2) Plateforme Nationale de Frittage Flash, PNF[2] CIRIMAT UMR 5085 CNRS/UPS/INPT, 118 route de Narbonne, 34062 Toulouse Cedex 4, France,
(3) Centre for Materials Science and Nanotechnology, University of Oslo, 1126 Blindern, NO-0318 Oslo, Norway
(4) University of Science and Technology (NTNU), Institut for Material Technology, Alfred Getzv. 2, 7491Trondheim, Norway

1. Introduction – State-of-the-art

Proton conducting electrolytes have many potential applications in electrochemical devices for hydrogen sensing, energy conversion, and hydrogen separation. High temperature proton conductors have attracted extensive attention as alternative electrolyte materials for solid oxide fuel cells (SOFC). In comparison to their oxygen ion conducting counterpart, protonic fuel cells would offer higher flexibility to various fuels and higher intrinsic thermodynamic efficiency [1,2]. In these fuel cells, water vapour is produced at the oxygen electrode, thus the fuel is not diluted and higher conversion efficiency may be reached [2,3]. Moreover, proton conductors may offer superior conductivities in an intermediate temperature region (300-500°C), and the slow reaction at the cathode of SOFCs based on oxygen conducting electrolytes is replaced by cathode and anode reactions expected to be faster. As a consequence, the working temperature of the proton conductor-based SOFC can be reduced, which is important for the materials stability and lifetime.

The most extensively studied proton conducting electrolytes are based on perovskite-type materials [4]. Combining high protonic conductivity with sufficient thermodynamic stability is a key issue for several of these materials, due to the formation of alkali-earth hydroxides and carbonates at low temperatures. Despite significant fundamental work to identify new improved materials only limited success has so far been achieved [5,6,7,8].

Among perovskite-type oxides, Ba-zirconates have shown good stability in CO_2-containing atmospheres. Moreover, these materials have recently been recognized to exhibit higher bulk conductivity than those of doped $BaCeO_3$ solid solutions, even exceeding the conductivity of the best oxide ion conductors at intermediate temperature (< 500°C) [9]. However, a high grain interior conductivity is counterbalanced by an apparently high grain boundary resistance whose origin is still not understood. A low mobility of protons or a low concentration stemming from e.g. space charge effects have been suggested [10], but the underlying causes are not clear.

A better understanding of this phenomenon is currently hampered by problems of controlling composition during densification as well as lack of systematic measurements reported in literature. The data on conductivity reported can vary with more than one order of magnitude. Therefore, much effort is still directed towards the

understanding of these materials as promising performance is expected from a decrease in grain boundary resistance.

In the search for novel proton conductors stable in CO_2/H_2O containing atmospheres, acceptor doped rare earth orthoniobates $LnNbO_4$ and tantalates $LnTaO_4$ have recently been demonstrated to exhibit proton conductivity in humid atmospheres, with only minor electronic conductivity [5,11]. The materials in this class exhibit monoclinic (fergusonite at low temperature) and tetragonal (scheelite at high temperature) structures, with transition temperature from around 500°C ($LaNbO_4$) and upwards. The phase transformation imposes thermal expansion changes, but the materials exhibit ferroelasticity, which improves their mechanical robustness.

The apparent solubility of alkaline earth cations is of the order of one mol% and a maximum proton conductivity of around 10^{-3} S/cm is obtained for such doped $LaNbO_4$. Impedance spectroscopy measurements have demonstrated that the overall proton conductivity in polycrystalline materials is limited by grain boundary resistance, which, nevertheless, appears to have less effect compared to that observed in some perovskite-type proton conductors. As for Ba-zirconate oxides which exhibit modest overall proton conductivity, the applicability of this new class of proton conductors requires the manufacturing of thin electrolyte films to meet economically interesting SOFC performance.

A variety of techniques have been extensively investigated aiming at the production of supported proton conducting thin films with a thickness of the order of 1-50 µm [12,13,14,15,16,17]. However, despite attractive features, the majority of these techniques are not cost-effective in large surface area production. Among the more promising processes, chemical solution deposition offers some advantages as easy composition control, easy fabrication of large surface area, and low heat treatment temperature. The drawback of this technique is that the dense films are produced with a thickness of a few hundred nanometers after a single coating which requires multiple coating steps (typically with additional heat treatment) in order to obtain stable defect free films. Manufacturing costs will be a challenge if too many processing steps are required in film fabrication.

An alternative is to use colloidal ceramic solutions, which allow coating of layers of few microns in a single step. The solutions consist of ceramic particles dispersed in organic or water-based media. The success of the particle deposition methods strongly depends on the characteristics of the powders as high sintering temperatures are often required to achieve fully densified electrolytes. Such high temperatures may lead to interfacial reaction between the supports and the electrolyte, phase decomposition, contamination, etc.

We aim at developing thin electrolyte materials with thickness below 10 µm. Investigation of the grain boundary resistance is therefore critical since such materials may consist of nano-size and submicro-size grains. By applying spark plasma sintering (SPS) to prepare $BaZr_{0.9}Y_{0.1}O_3$ from nano-size powder, we have produced dense electrolytes within a few minutes. The short sintering time reduced grain growth enabling us to compare the conductivity of materials with different grain sizes. Furthermore, a manufacturing process for the production of fuel cells with thin electrolytes (≤10 µm) was successfully developed. It comprises spray-pyrolysis for production of oxide nanoparticles, and application of deposition methods for production of the different functional layers. The flexibility of this process will be

illustrated through the production of several single SOFC cells with $BaZr_{0.9}Y_{0.1}O_3$ and $La_{0.995}Sr_{0.005}NbO_4$ electrolytes [5,9 ,18,19].

2. Experimental

2.1. Spark Plasma Sintering of $BaZr_{0.9}Y_{0.1}O_3$ ceramics

In our experiments, the SPS graphite die was filled with the raw material powder (without any additives or sintering aids), and was placed between two electrodes (lower and upper). The upper electrode was fixed while the lower one was mobile and allowed applying a uniaxial pressure (along z axis) to the die. In order to protect the die from powder contamination, a protective conductive sheet such as a papyex paper (made of carbon) was applied.

$BaZr_{0.9}Y_{0.1}O_3$ (BZY) spray-pyrolysed powder was produced as described elsewhere [20]. The powder was sintered as disks of 15 mm diameter and ~ 2 mm thickness by SPS using a Dr. Sinter 2080 apparatus (Sumitomo Coal Mining Co., Tokyo, Japan). The powder was poured in a graphite die, heated at 200°C/min up to the sintering temperature (1600°C, 1650°C) with increasing pressure up to 100 MPa applied from 600 or 650°C. A dwell of 5-15 min was used at the sintering temperature. During cooling, the electrical power was switched off and the cooling to room temperature was achieved in 10 minutes.

Sintered disks were annealed in air at 700°C for 2 hours to remove carbon deposits from the SPS apparatus. Samples were then characterized by light microscopy, X-ray diffraction (XRD) (Siemens D710 diffractometer), scanning electron microscopy (SEM) (JEOL JSM-5900LV SEM) and electron probe microanalysis (EPMA) (Cameca SX100).

The disk conductivity was measured by impedance spectroscopy in humid oxygen atmosphere (2% H_2O). The specific grain boundary conductivity was interpreted using the brick layer model.

2.2. Production of single cells

2.2.1 Synthesis and characterization of spray-pyrolysed powders

Electrolyte materials ($La_{0.995}Sr_{0.005}NbO_{4-\delta}$ (LSNb), $BaZr_{0.9}Y_{0.1}O_{3-\delta}$ (BZY)) and cathode materials ($CaTi_{0.9}Fe_{0.1}O_{3-\delta}$ (CTF), $La_2NiO_{4+\delta}$ (LNi)) were synthesized by spray-pyrolysis according to a method described elsewhere [20].

Powder phase purity was characterized by XRD analysis. Powder mean grain size was characterized by SEM.

2.2.2. Preparation and characterization of fuel cells

LSNb-NiO anode supports were prepared by first mixing LSNb and NiO powders and then tape casting a slurry made from this mixture. Corn starch filler was added to the slurry for controlling porosity. This preparation is thoroughly described elsewhere [21].

The slurries were cast onto a Milar^{TM} film and left drying overnight at room temperature in a closed box. Dried tapes were laminated at 45°C with a pressure of 5 tons for 30 s. Green bodies of laminated tapes, 20 mm in diameter, were heated up to 550°C at a heating rate of 10°C/h and held for 10 hours to slowly remove all organic additives. They were then annealed at 1000°C for 2 hours to achieve sufficient strength for supporting the electrolyte.

Colloidal suspensions were prepared by dispersing BZY and LSNb powders in a mixture of methylethylketone and terpineol (60/40 % vol.). Polyvinylbutyral (Butavar B-98) binder (0.03 % wt) was also added in order to reach an appropriate viscosity of about 25 mPa.s. The suspensions were prepared with 13 wt % of solids loading and homogenised for 2 hours in a planetary mill at 360 rpm.

BZY or LSNb suspensions were spin-coated one time onto the LSNb//NiO anode support with a spinning speed of 2000 rpm for 30 s. Half-cells (electrolyte + anode) were sintered in air at 1350°C for 2 hours.

For the deposition of the cathodic layers by screen-printing, CTF and LSNb/LNi (60/40 % vol.) inks were prepared by mixing in a planetary mill a commercial organic vehicle (HVS006, Heraeus, GmbH, Hanau), the ceramic powder (38 % in wt.) and a few droplets of terpineol. Single cells (cathode top layer on electrolyte layer on anode support) were annealed in air at 1100°C for 2 hours.

Reduction of anodic electrodes was performed in a mixture of 10% H_2/Ar with 2% water vapour at 900°C for 3 hours.

Cell composition and texture were studied by XRD, EDS and SEM analyses. Gas tightness of the electrolytes was examined at ambient temperature by measuring helium leakage. Anode porosity was evaluated by Archimedes methods in water.

3. Results and discussion

3.1. Spark Plasma Sintering of BZY ceramics

3.1.1. SPS features

SPS is a relatively new sintering technique, featuring the capability of sintering metal and ceramic powders quickly to high density at reduced temperature. According to the inventor of this technique, the external power source provides pulsed discharges that clean and activate the surface of the contacting particles [22,23]. Through charging and discharging the space between powder particles with electrical energy, high temperature spark discharge/plasma is momentarily generated and facilitates sintering [24,25,26]. SPS may readily consolidate powders under uniform heating. The short operation time, typically a few minutes, minimizes grain-growth, thus enabling the production of nanophase dense ceramics. This short operation time may also reduce the evaporation of volatile compounds, for instance Sr or Ba.

3.1.2. Production of BZY ceramics by SPS

In order to prepare sintered materials with different grain sizes, BZY samples were consolidated using the different protocols reported in table 1.

Four samples (SPS 1-4) were sintered using conventional SPS procedures (use of heat and pressure) whereas two others underwent specific features:

- one BZY sample (SPS 5) was sintered at 1650°C for 5 min, turned upside-down and sintered once more using similar processing conditions

- one BZY sample (SPS 6) was sintered with a alumina powder bed poured into the graphite die and placed in contact with the positive electrode. To prevent BZY contamination by alumina, a papyex sheet was placed in between the two powders.

SPS consolidated BZY was single phase as shown by the XRD patterns reported in Fig. 1. Patterns have been recorded on both sides of each sample and no difference was detected. The lattice parameter of the BZY cubic phase was between

4.204 Å and 4.206 Å, and in good agreement with that measured on BZY spray-pyrolysed powder (4.207 Å), and reported in the literature [27,28].

Table 1: SPS procedures for BZY samples

Samples	Conditions of sintering	Density (%)
SPS 1	1600°C 5 min	95
SPS 2	1650°C 5 min	97
SPS 3	1600°C 15 min	96
SPS 4	1650°C 15 min	98
SPS 5	Sintered two times at 1650°C 5 + 5 min - turned upside-down	98
SPS 6	1650°C 5 min Alumina powder bed placed on electrode (+)	97
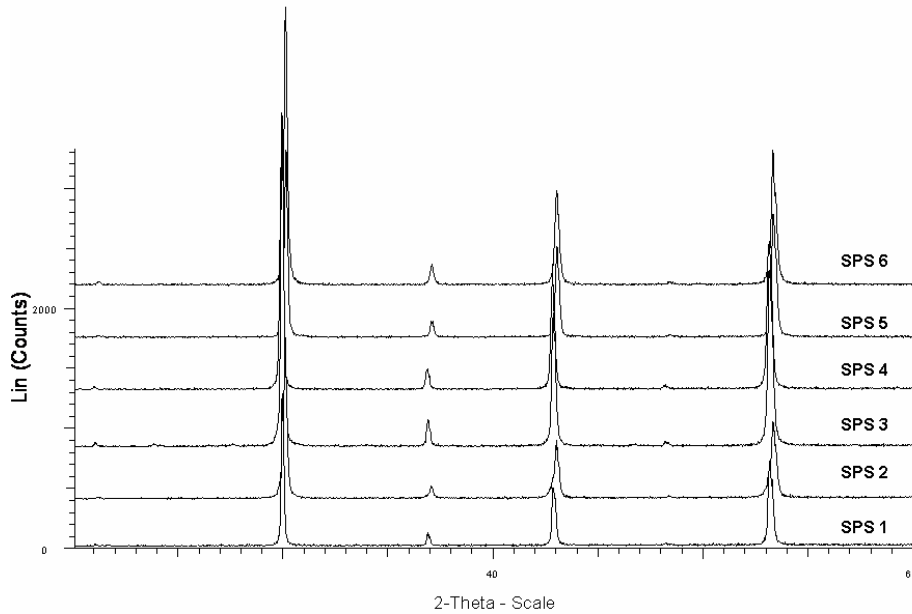
Fig. 1: XRD patterns of SPS consolidated BZY ceramics

SPS processing parameters were investigated by comparing the microstructure and density (calculated using a theoretical density for BZY of 6.21 g.cm^{-3}). All samples have a fairly high density above 95% (table 1). The lowest density was observed for sample SPS 1 sintered at 1600°C for 5 min, which exhibits small pores and a grain size of about 130 nm (Fig. 2 a). This grain size is comparable to that measured for powder particles (Fig. 9d), indicating that no grain growth occurred during the SPS densification. Increasing the temperature up to 1650°C (SPS 2) led to an increase in the grain size to 200 nm and simultaneously, an increase in density to 97% (Fig.2b).

The use of alumina powder in order to create an insulating layer between BZY and the electrodes, did not appear to have any significant effect on the density of SPS sample, which can be seen by comparing SPS 6 and SPS 2 (Fig. 3 and 4).
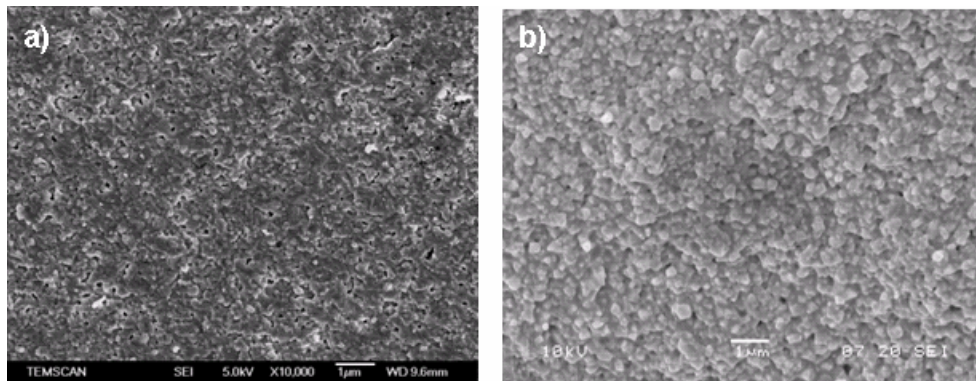
Fig. 2: SEM micrographs of SPS BZY consolidated ceramics after sintering at a) 1600°C – 5min and b) 1650°C 5 min

Effects of the different sintering protocols on composition were also investigated by light microscopy. For instance, Fig. 3 illustrates the results obtained on sample SPS 2 using both bright and dark fields. For comparison, SEM micrograph is also reported.
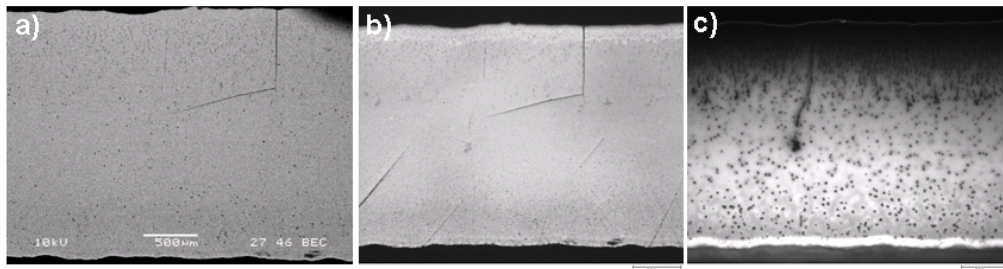
Fig. 3: a) SEM micrograph and b) light microscopy pictures taken with bright field and c) with dark field of SPS 2 sample of BZY

The SEM analysis (Fig. 3a) revealed that the SPS 2 sample was fully dense and contained a small amount of carbon, which may not exceed 3% according to sample density (table 1). This carbon contamination is also evidenced from light microscopy using bright field (Fig. 3b) and even more from dark field image (Fig. 3c).

C intrusion pattern of SPS 2 can be described as a dark front layer of about 200 µm thickness deep into the ceramic from the surface in contact with the negative electrode. This front is extended by long strings of small C inclusions, indicating that C migrates from the upper surface. Differently, the other side of the sample in contact with the positive electrode exhibits a bright layer with no trace of C. This oriented C pattern indicates that the C diffusion is controlled by the electrical field. This assumption is supported by the comparison of samples SPS 2 and SPS 6 sintered at the same temperature with similar sintering period (Fig. 4). The use of alumina during sintering of SPS 6 seems to reduce C diffusion, as the upper side of the sample exhibits a much thinner dark layer compared to SPS 2.

It is also interesting to notice that all SPS samples exhibit small inclusions of C trapped in the ceramics bulk.
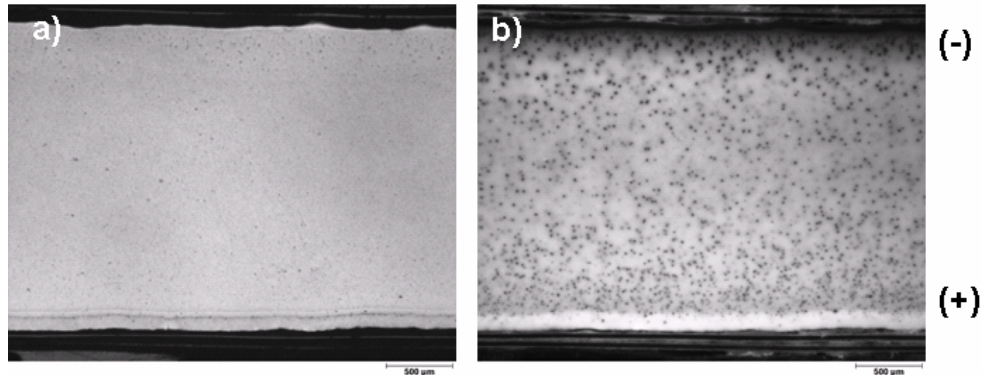
Fig. 4: Pictures of SPS 6 sample obtained by light microscopy using a) bright field and b) dark field. Positions of electrodes are indicated by (+) and (-) symbols

C-contamination by C intrusion on the top side of SPS consolidates may originate from die contamination. The SPS set-up provides a reducing atmosphere at high temperature which could lead to carbon evaporation from carbon-containing sources. It has already been suggested that the plasma generated in the SPS process may activate C atoms and favour reaction-diffusion of C into the powder materials [29].

The presence of small C inclusions in bulk ceramics may also originate from the powder (e.g. carbonates on the surface demonstrated by infra-red spectroscopy). Fast surface densification could occur if heat conduction is low, which may result in trapping of carbon from decomposition of the powder.

Samples composition was studied by EPMA analysis through the surface and the whole thickness of each sample. The elemental diffusion profile determined from these analyses confirmed that the composition of all ceramics was homogeneous (Fig. 5).
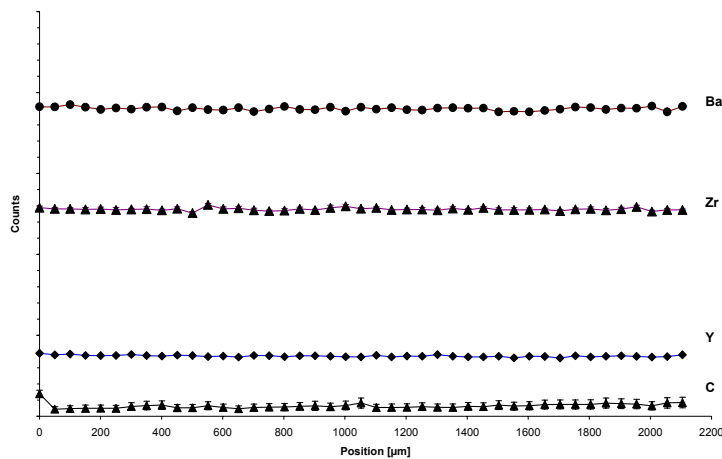
Fig. 5: Elemental diffusion profiles determined from EPMA analysis on SPS samples

It is worthwhile to notice that despite the apparently strong variation of C amount from light microscopy analyses, C concentration inside SPS samples remained constant over the whole thickness. This indicates that the size distribution of C inclusions is varying in different regions of the ceramic cross-section (see Fig. 4b).

Impedance spectroscopy measurements performed in humid oxygen on sample SPS 1 are illustrated in Fig. 6. The measurements showed that the specific grain boundary resistance obtained using the brick-layer model approach is higher compared to that in the grain interior, by nearly 4 orders of magnitude.

The grain interior conductivity is in good agreement with data reported in literature on polycrystalline samples densified by other processes. The specific grain boundary resistance is fairly high, of about 3.10^{-7} S/cm at 500°C, which probably reflects the small grain size in the SPS sample.
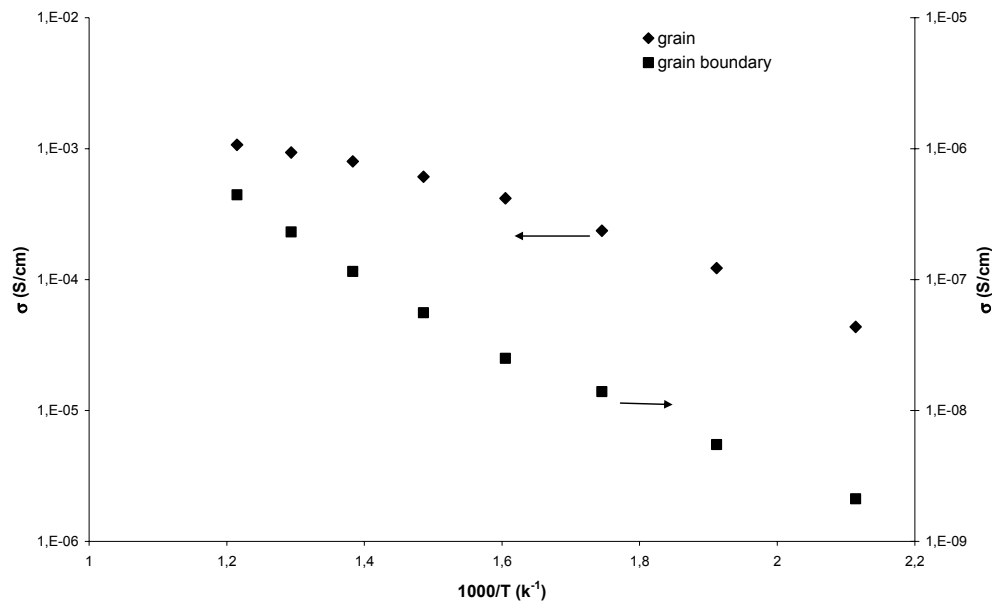
Fig. 6: Specific grain and grain boundary conductivities from impedance spectroscopy vs. 1/T in wet O$_2$.

3.2. Production of single unit cells

Many studies have been carried out to prepare efficient ceramic proton conducting fuel cells but performance typically do not exceed the stated commercial target of 100 mW/cm^2 at 600°C at 700 mV [8,30,31,32,3,33]. Provided that thinner electrolyte and electrodes with improved performance can be manufactured, an increase in cells current densities may be achieved [2,31]. Regarding electrodes performance, it has been widely demonstrated in SOFCs that electrochemical reaction kinetics both at the cathode and the anode depend on materials intrinsic properties as well as on microstructure. Preparation of graded or composite electrodes would promote higher active surface area, better pathways for ionic diffusion and longer triple-phase boundary length [34,35]. An objective of the work was therefore to develop a cost-effective manufacturing process meeting these requirements. Therefore, BZY or LSNb electrolytes supported on LSNb//Ni cermet anodes have been coated by thin

cathode layers of LNi//LSNb composite or CTF to produce single unit cell. LNi has shown to exhibit among the highest surface exchange and oxygen diffusion kinetics of perovskite-derived materials [36].

3.2.1. Spray-pyrolysed powders characteristics

XRD and SEM analyses revealed that spray-pyrolysed powders were single phase and consisting of agglomerated nano-sized (LSNb and BZY) and sub-micron (CTF and LNi) primary particles (Fig. 7). Powders characteristics giving their phase structure, particle size and bulk density are reported in table 2.
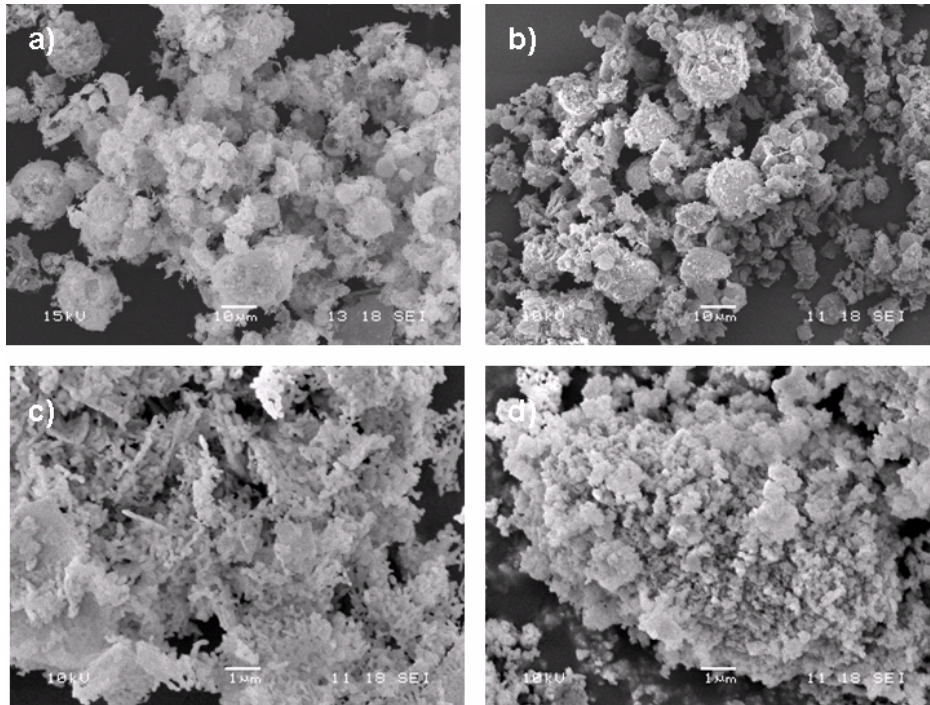
Fig.7. SEM micrographs of a) LNi, b) CTF, c) LSNb and d) BZY powders

Table 2: Characteristics of spray-pyrolysed powders

	LSNb	BZY	CTF	LNi
Structure at room temperature	Fergusonite	Perovskite	Perovskite	Ruddlesden-Popper
Mean particle diameter (± 20 nm)	100 nm	150 nm	500 nm	500 nm
Theoretical density	5.9 g/cm^3	6.21 g/cm^3	4 g/cm^3	7 g/cm^3

3.2.2. Fuel cells characteristics

Fig. 8 shows that SEM micrographs of LSNb electrolyte coated on LSNb//NiO anode (half-cell) after sintering at 1350°C.
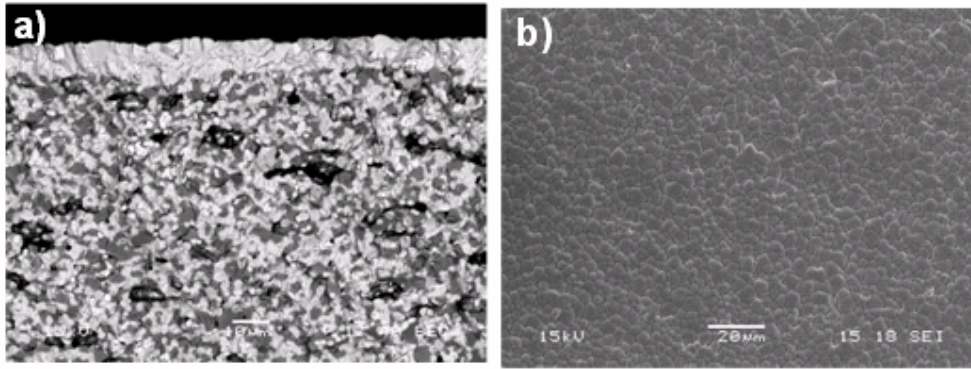
Fig. 8. SEM micrographs of a) cross-section of sintered (with non-reduced anode) half-cell (anode + electrolyte) and b) LSNb electrolyte surface

Sintering at 1350°C results in a shrinkage of about 36% and a fully dense LSNb electrolyte with a thickness of 10 µm. EDS and SEM analyses indicated that both the electrolyte and the anode were homogeneous in composition and that no interface reaction had occurred. XRD analysis performed on the materials confirmed this. Furthermore, no He-leakage was detected by gas chromatography indicating that electrolyte layer was defect free.

A SEM micrograph of a BZY half-cell is shown in Fig. 9. The BZY electrolyte coated onto the LSNb//NiO anode and sintered at 1350°C is fully dense and defect free. This result is promising considering data reported in literature, which usually referred to temperatures above 1500°C for achieving a fully dense BZY electrolyte [37,38]. This may be attributed to the sintering behaviour of LSNb//NiO anodes, which shrinks significantly during annealing at 1350°C. This could result in a high compressive stress facilitating densification of the electrolyte layer.
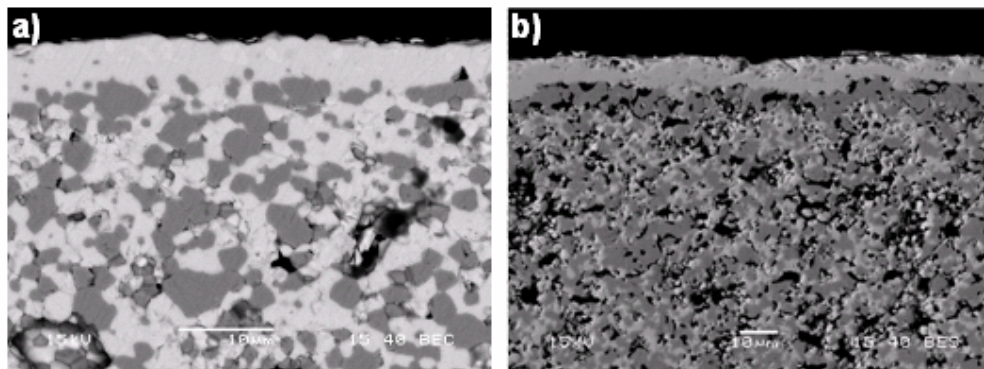
Fig. 9. SEM micrographs of sintered BZY electrolytes half-cells a) before reducing LSNb//NiO anode in H_2 containing atmosphere, b) after reducing the anode in H_2 containing atmosphere

LSNb and BZY half-cells were characterised by XRD and SEM/EDS analyses after annealing the cells in a mixture of 10% H_2/Ar with 2% water vapour at 900°C for 3 hours. XRD analyses did not reveal any effect of this treatment on the phase structure of the electrolyte material and confirmed that NiO oxide was reduced to Ni

metal (Fig. 10). This reduction resulted in an increase in the anode open porosity, which is considered to be caused by the volume change on converting nickel oxide to Ni. After reduction, the anode porosity was about 40 % with small pores of about 0.2 µm diameter and larger ones of about 7 µm, the latter resulting from the pyrolyse of corn starch filler.
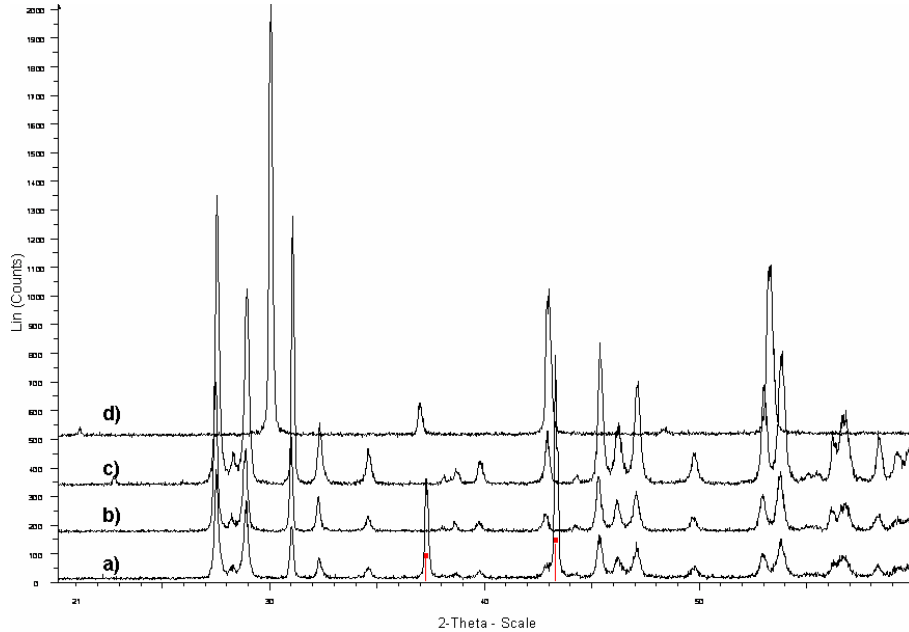
Fig. 10. XRD patterns of a) LSNb//NiO anodes, b) LSNb//Ni anodes after reduction in H$_2$ atmosphere, c) LSNb electrolyte after reduction and d) BZY electrolyte after reduction

Single unit cells with screen-printed cathodes are shown in Fig. 11. Monophase and composite cathodes were porous, crack-free and adherent to the electrolytes with a thickness of about 20 µm. No interfacial reaction or delamination was observed.
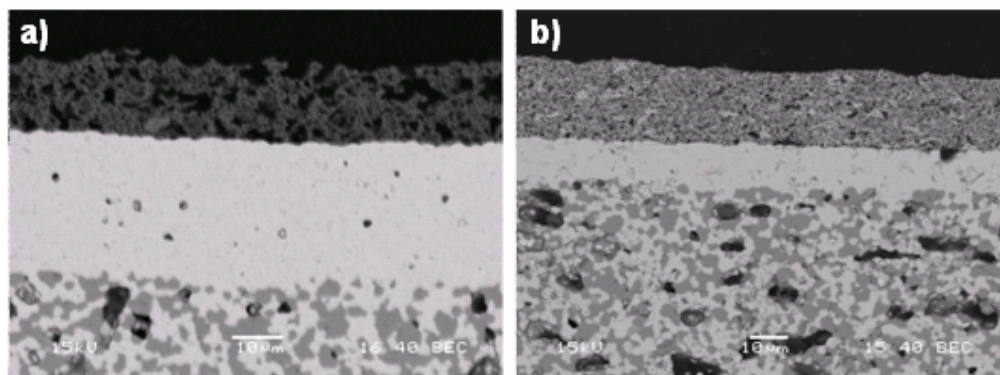
Fig. 11. SEM micrographs of fuel cells with LSNB electrolyte and screen-printed a) CTF monophase cathode and b) LSNb//LNi composite cathode

Further investigations of these fuel cells are in progress and will be reported elsewhere.

CONCLUSIONS

A novel sintering technique termed spark plasma sintering has been applied for controlling the grain growth in the BZY electrolyte and for the study of grain boundary resistance. Spark plasma sintering allowed densification of BZY in short operation times (less than 30 min). Preliminary results obtained from conductivity measurements indicate that the grain conductivity is in agreement with previously reported data, and that grain boundary resistance in the nanophase electrolyte is fairly high. Further experiments are in progress to complete this study.

A reliable and cost-effective process has been successfully developed for the preparation of solid oxide fuel cells with proton conducting electrolytes. This process combines three reliable techniques namely tape-casting, spin-coating and screen-printing which are reproducible, easily up-scalable and versatile. Process flexibility allows controlling electrodes porosity and architecture as well as electrolyte thickness down to a few microns. This process appears to be of potential interest for the preparation of ceramic layered devices which can be used in fuel cells and hydrogen separation technologies. Work is currently in progress to scale up the size of the fuel cells.

References

[1] N.Q. Minh, T. Takahashi, Science and Technology of Ceramic Fuel Cell, Elsevier, Amsterdam (1995)

[2] W.G. Coors, J. of Power Sources, 118 (2003) 150

[3] P. Ranran, W. Yan, Y. Lisia, M. Zongqiang, Solid State Ionics, 177 (2006) 389

[4] T. Takahashi, H. Iwahara, Rev. Chim. Miner.,17 (1980) 243

[5] T. Norby, R. Haugsrud, R.A. Strøm., T. Grande, K. Wiik, M.-A. Einarsrud, Patent application (2005)

[6] K.D. Kreuer, S. Adams, W. Münch, A. Fuchs, U. Klock, J. Maier, Protonic conducting alkaline earth zirconates and titanates for high drain electrochemical applications, Solid State Ionics, 145 (2001) 295

[7] H. Iwahara, Y. Asakura, K. Katahira, M. Tanaka, Solid State Ionics, 168 (2004) 299

[8] N. Bonanos, K.S. Knight, B. Ellis, Solid State Ionics, 79 (1995) 161

[9] K.D. Kreuer, Solid State Ionics, 125 (1999) 285

[10] P.I. Dahl, PhD Thesis, Dept. of Materials Science and Technology, NTNU, Trondheim, Norway (2006)

[11] R. Hausgrud, T. Norby, Nature Materials, 5 (2006) 193

[12] C. Xia, T.L. Ward, P. Atanasova, R.W. Schwartz, Journal of Materials Research, 13 (1998) 173

[13] G.Y. Meng, H.Z. song, H.B. Wang, C.R. Xia, D.K. Peng, Thin Solid Films, 409 (2002) 105

[14] H. Itoh, H. Asano, K. Fukuroi, M. Nagata, H. Iwahara, Journal of American Ceramic Society, 80 (1997) 1359

[15] Q. Zhu, B. Fan, Solid State Ionics, 176 (2005) 889

[16] T. Schneller, T. Schober, Solid State Ionics, 164 (2003) 131

[17] S. Cheng, V.K. Gupta, J.Y.S. Lin, Solid State Ionics, 176 (2005) 2653

[18] A. Sin, B. El Montaser, P. Odier, J. of Am. Ceram. Soc., 85 (2002) 1928

[19] U. Anselmi-Tamburini, M.T. Buscaglia,M. Viviani, M. Bassoli, C. Bottino, V. Buscaglia, P. Nanni, Z.A: Munir, J. of Eur. Cer. Soc., (2005) in press, available online

[20] T. Mokkelbost et al., "High temperature proton conducting $LaNbO_4$-based materials. Part I: Powder synthesis by spray pyrolysis", to be submitted (2006)

[21] M.L. Fontaine, J. Smith, Y. Larring, K. Wiik, H. Raeder, R. Bredesen, Proceeding of ICIM9, Lillehammer, Norway 20 – 24 July (2006)

[22] Inoue (K.), US Patent, N° 3 241 956 (1966)

[23] Inoue (K.), US Patent, N° 3 250 892 (1966)

[24] http://www.scm-sps.com/e_htm/whatsps_e_htm/whatsps4_e.htm

[25] M. Omori, Materials Science and Engineering A 287 (2000) 183.

[26] M. Nygren, Z. Shen, Solid State Science 5 (2003) 125.

[27] T. Schober, H. G. Bohn, Solid State Ionics, 127 (2000) 351-360

[28] K. Katahira,Y. Kohchi, T. Shimura, H. Iwahara, Solid State Ionics, 138 (2000) 91-98

[29] L.G. Yu, K.A. Khor, H. Li, k.C. Pay, T.H. Yip, P. Cheang, Surface and Coatings Technology, 182 (2004) 308

[30] W.G. Coors, Proc. 5th European Solid Oxide Fuel Cell Forum 2 (2002) 602

[31] S. Yamaguchi, T. Shishido, H. Yugami, S. Yamamoto, S. Hara, Solid State Ionics, 162-163 (2003) 291

[32] H. Iwahara, Solid State Ionics, 77 (1995) 289

[33] T. Schober, Solid State Ionics, 162-163 (2003) 277

[34] G.C. Mather, F.M. Figueiredo, D.P. Fagg, T. Norby, J.R. Jurado, J.R. Frade, Solid State Ionics, 158 (2003) 333

[35] T.L. Ngyuen, K. Kobayashi, T. Honda, Y. Iimura, K. Kato, A. Neghisi, K. Nozaki, F. Tappero, K. Sasaki, H. Shirahama, K. Ota, M. Dokiya, T. Kato, Solide State Ionics, 174 (2004) 163

[36] F. Mauvy, C. Lalanne, J.M. Bassat, J.C. Grenier, H. Zhao, P. Dordor and Ph. Stevens, Journal of the European Ceramic Society, Volume 25, Issue 12 (2005) 2669

[37] F.M.M. Snijkers, A. Buekenhoudt, J. Cooymans, J. J. Luyten, Scripta Materialia, 50 (2004) 655

[38] T. Schober, H. G. Bohn, Solid State Ionics, 127 (2000) 351